PCCP

PAPER

View Article Online
View Journal | View Issue

Cite this: *Phys. Chem. Chem. Phys.*, 2015, **17**, 23602

Hyperconjugation in diethyl ether cation *versus* diethyl sulfide cation†

Masato Morita,‡[a] Yoshiyuki Matsuda,*[bc] Tomoya Endo,[b] Naohiko Mikami,[b] Asuka Fujii[b] and Kaito Takahashi*[a]

Received 30th June 2015,
Accepted 3rd August 2015

DOI: 10.1039/c5cp03765d

www.rsc.org/pccp

Ionization of a molecule can greatly alter its electronic structure as well as its geometric structure. In this collaborative experimental and theoretical study, we examined variance in hyperconjugation upon ionization of diethyl ether (DEE) and diethyl sulfide (DES). We obtained the experimental gas phase vibrational spectra of DEE, DES, DEE^+, DES^+, DEE^+–Ar, and DES^+–Ar in the wavenumber region of 2500 to 3600 cm^{-1}. For DEE^+ and DEE^+–Ar, we observed a greatly red shifted CH stretching peak at 2700 cm^{-1}, while the lowest CH stretching peaks for DEE, DES, DES^+ and DES^+–Ar were observed around 2850 cm^{-1}. For DEE^+, we calculated a drastic red shifted CH stretching peak at 2760 cm^{-1}, but for DEE, DES, and DES^+ the lowest CH stretching peaks were calculated to be at 2860, 2945, and 2908 cm^{-1}, respectively. In addition, for DEE, the minima (maxima) geometry in the neutral state becomes a maxima (minima) geometry in the cationic state, while similar minima geometries are seen in neutral and cationic states of DES. These experimental and theoretical findings were rationalized through the natural bond orbital analysis by quantifying the hyperconjugation between the σ_{CH} orbital and the ionized singly occupied p orbital of the oxygen (sulfur) in DEE^+ (DES^+). This study showed how orientation with the ionized orbital can greatly affect the neighboring CH bond strength and its polarity, as well as the geometry of the system. Furthermore, this change in the CH bond strength between DEE^+ and DES^+ is quantified from the energies for intramolecular proton transfer in the two cations.

I. Introduction

Seventy-five years ago, Mulliken and coworkers coined the term "hyperconjugation" to describe the interaction arising from the delocalization of the σ electron to a neighboring π* orbital.[1,2] This concept has been used and generalized to understand stability and reactivity of many chemical systems.[3] For example, the preference of the staggered conformation for ethane has been discussed as a hyperconjugation interaction between the occupied σ_{CH} orbitals of one methyl group and anti-bonding σ^*_{CH} orbitals of the another methyl group, namely a $\sigma \rightarrow \sigma^*$ interaction.[4–8] Furthermore, discussion on the relationship between the anomeric effect of monosaccharides and hyperconjugated delocalization from oxygen lone pairs to the vacant anti-bonding σ*, the $n \rightarrow \sigma^*$ interaction, has also attracted great attention.[9] In addition, Saunders has mentioned the importance of negative ion hyperconjugation for the carbanion elimination reactions.[10,11] Recently, Meloni *et al.* have reported that most alkylic peroxy radicals dissociatively ionize due to fragment stabilization by hyperconjugation.[12,13] Changes in bond lengths, dipole moments, bond dissociation energies and heats of formation have been mentioned as consequences of hyperconjugation.[14–18]

Vibrational spectroscopy of XH stretching bonds, where X = C, N, O, *etc.*, has attracted researchers as markers to understand the local environment of the XH bond. For example, red shifts and increases in intensities of the XH stretching fundamental spectra are usually associated with hydrogen bond formation, where the

[a] *Institute of Atomic and Molecular Sciences, Academia Sinica, P. O. Box 23-166, Taipei, 10617 Taiwan, Republic of China. E-mail: kt@gate.sinica.edu.tw; Tel: +886-223668237*

[b] *Department of Chemistry, Graduate School of Science, Tohoku University, Armaki-Aoba, Aoba-ku, Sendai 980-8578, Japan. E-mail: matsuda@m.tohoku.ac.jp; Tel: +81-22-795-6573*

[c] *Institute for Excellence in Higher Education, Tohoku University, Kawauchi 41, Aoba-ku, Sendai, 980-8576, Japan*

† Electronic supplementary information (ESI) available: Details concerning the energetics and multidimensional vibrational calculations; a table summarizing the CH stretching vibrations using the local mode model for neutral ag diethyl sulfide (DES); four tables comparing the LM model *versus* the LM(NM)-4D model for aa diethyl ether (DEE) and gg, gg′, and sg DEE^+; a table comparing the relative energies for DEE^+–Ar; a figure showing the two-dimensional potential energy surface of DEE^+; a figure showing the schematic geometry of DEE^+–Ar; a figure showing the vibrational modes of DEE^+; a figure comparing the methyl torsion angle dependence of the C3H9 stretching peak position; a figure comparing the COCH torsion angle dependence of the C3H9 stretching vibrational peak intensity; and Cartesian geometries optimized by the MP2/6-311++G(3df,3pd) method. See DOI: 10.1039/c5cp03765d

‡ Present address: Department of Chemistry, Durham University, South Road, Durham DH1 3LE, UK.

XH bond is donating to an acceptor Y atom in the XH···Y form.[19–23] However there have been several cases for cations where red shifts and increases in intensities of CH bonds have been observed in situations where hydrogen bonding is not present. These cases have been rationalized through the concept of hyperconjugation.[24–29] When a σ_{CH} orbital interacts with an empty neighboring π orbital through hyperconjugation, the electron density in the CH bond decreases. Thus, the CH bond weakens, causing a red shift from the usual CH stretching peak seen at around 3000 cm^{-1}. Furthermore this decrease in electron density also causes the CH bond to become more polarized and this is observed through the massive increase in the absorption intensity. Therefore, hyperconjugation can greatly alter the electronic distribution of the CH bond in cations. For hydrocarbon cations such as toluene[24] and *tert*-butyl cations,[25] previous experiments have observed very intense peaks at 2863 and 2834 cm^{-1}, respectively. They have been attributed to the hyperconjugation of the σ_{CH} orbital to the π^*_{CC} orbital. Recently, large red shifts of the CH stretching peaks were reported for methanol[26] and diethyl ether cations[27] $CH_3CH_2OCH_2CH_3^+$ (DEE^+). For DEE^+, theoretical calculations showed that this is attributed to a very strong hyperconjugation of the σ_{CH} orbital and the adjacent ionized oxygen p singly occupied molecular orbital (SOMO). The increase in red shift for DEE^+ compared to the toluene cation can be rationalized as due to the strong electron-withdrawing ability of the ionized oxygen atom compared to the carbon in the benzene ring. We note that this feature is different from that of neutral DEE where "negative" hyperconjugation occurs through the back donation of electrons from the nonbonding oxygen orbitals to the antibonding σ^*_{CH} orbital.[28–31] In this paper, we extend the experimental and theoretical studies to the diethyl sulfide cation, $CH_3CH_2SCH_2CH_3^+$ (DES^+), where the oxygen is exchanged with a sulfur atom. The key question is whether the more diffuse 3p orbital of sulfur results in a stronger hyperconjugation compared to oxygen or not. Furthermore, to obtain a deeper understanding of the effect of hyperconjugation in these RXR systems where X = O or S, we theoretically compared the differences in the potential energy surfaces and vibrational spectra of the two molecules in detail.

On the experimental side, this study was performed using infrared (IR) spectroscopy based on the vacuum-ultraviolet (VUV) photoionization detection. This spectroscopic method enables us to carry out detection of both neutral and cationic DEE and DES by varying the firing of the IR laser before and after VUV one-photon ionization, respectively. We observed the IR spectra of both the neutral and the cationic DEE and DES. On the theory side, we performed quantum chemistry calculations to obtain stable conformers of DEE, DEE^+, DEE^+–Ar, DES and DES^+. The local mode model vibrational calculations as well as their multi-dimensional variants were performed for the CH bonds to obtain theoretical vibrational spectra to compare with the aforementioned experimental results. In addition, to investigate the ionization dynamics of DEE and DES, we performed on-the-fly direct dynamics using B3LYP. These results were further analyzed using a two-dimensional potential energy surface calculated by the aforementioned quantum chemistry methods. Then, natural bond orbital analysis of Weinhold and coworkers[32,33] was used to rationalize the differences between DEE^+ and DES^+ and its correlation with hyperconjugation. Lastly, the possibility of intramolecular proton transfer for these cations was evaluated.

The rest of the paper is organized in the following manner. In Section II, the details of the experimental and theoretical methods are given. In Section III, we present the detailed analysis of the experimental results using the theoretical calculations. Lastly, we provide a brief conclusion in Section IV.

II. Experimental and theoretical methods

A. Experimental methods

Details of the experimental setup have been written elsewhere.[34] Jet-cooled DEE or DES was ionized by VUV photoionization at 118 nm. In IR spectroscopy of the neutral state, the molecule was irradiated by IR light before VUV photoionization and the IR frequency was scanned. IR absorption was observed as an enhancement of ion intensity in a fragment mass channel through IR predissociation of the parent ion under investigation using a time-of-flight mass spectrometer. The 118 nm light was generated by third harmonic generation of the 355 nm output of an Nd:YAG laser (Continuum, Surelite-III) operated with a Xe–Ar (1 : 10) gas mixture. IR light was generated by differential frequency generation of the 532 nm output of an Nd:YAG laser (Continuum, Powerlite-8010) and the dye laser output (Continuum, ND-6000) operated with the DCM dye methanol solution. The sample concentration was controlled to prevent contaminations originating from clusters.

Helium was used as the carrier gas for IR spectroscopy of the bare DES^+, while DES^+–Ar was generated through the expansion of DES with Ar. IR spectroscopy of the bare DES^+ was carried out by delaying the injection of IR light with the same setup for the neutral state. On the other hand, the IR spectrum of DES^+–Ar was observed using a tandem-type quadrupole mass (Q-mass) spectrometer. In this setup, DES^+–Ar was selected through the first Q-mass. IR light was irradiated at the size-selected DES^+–Ar in the octupole ion guide region. The IR spectrum of DES^+–Ar was obtained by monitoring the fragment ion originating from vibrational predissociation of DES^+–Ar through the second Q-mass. The IR spectra of DEE and DEE^+–Ar are the same as those reported previously. They were observed using a tandem-type Q-mass spectrometer.[27,34] In the spectroscopy with the tandem-type Q-mass, IR light generated by an IR optical parametric oscillator (LaserVision) was used.

B. Quantum chemistry methods

First, we obtained the equilibrium geometries for the singlet ground electronic states of neutral DEE and DES using the B3LYP[35,36]/6-31++G(d,p),[37–40] B3LYP/6-311++G(3df,3pd), PBE0[41–43]/6-31++G(d,p), PBE0/6-311++G(3df,3pd) and MP2[44]/6-311++G(3df,3pd) methods. Then we performed the geometry optimization for the doublet states of DEE^+ and DES^+ using the unrestricted variant of the aforementioned methods to obtain all the structural conformers

for the cations. Lastly, using the optimized MP2 geometries, we performed a single point energy calculation by the UHF based UCCSD(T)[45–48] method to benchmark the validity of the calculated density functional calculation results. After confirming the validity of the methods, we used B3LYP, PBE0 and MP2 to calculate a two-dimensional torsion potential energy surface of the ethyl group rotation to rationalize the experimental results. Furthermore, to understand the dynamics following the ionization of neutral DEE and DES, we also performed on-the-fly direct trajectory simulation[49] using B3LYP/6-31++G(d,p).

In addition, the Ar-tagged 1 : 1 complex, DEE^+–Ar, was also calculated using the MP2 method. We obtained a total of 11 different DEE^+–Ar conformers for 4 different bare conformers of DEE^+. As given in the ESI,† Fig. S2 and Table S11, MP2 predicts that for DEE^+, Ar tends to bind to the tip of the CH bond, and the binding energy of ~0.08 eV does not vary with different conformers. Thereby the relative energies of the Ar-tagged complex follow the bare system and we will perform detailed analysis on the bare cations.

To understand the electron interaction responsible for the large CH stretching red shift seen for DEE^+, the natural bond orbital (NBO) analysis of Weinhold *et al.*[33] was performed using the B3LYP/6-31++G(d,p) wavefunction. All the calculations were performed using the Gaussian 09 program,[50] and all the stable Cartesian geometries optimized by the MP2 method are given in the ESI.†

C. Vibrational calculation

Since we are interested in the CH stretching vibrational peaks, we can resort to the local mode model, which has shown great success in the calculation of XH stretching spectra where X = O, C, N, *etc.*[51–58] In the actual calculation, we solved the one-dimensional vibrational Schrödinger equation for the CH stretching coordinate using the discrete variable representation[59] of the harmonic oscillator basis functions reported previously by some of the authors.[60,61] For each CH bond, 16 single point B3LYP/6-31++G(d,p) calculations were performed (R_{CHeq} − 0.5 to R_{CHeq} + 0.8 Å), and fourth order interpolation was used to provide the values of the potential energy and dipole moment for vibrational calculations. We note that since we are directly calculating the potential energy and dipole moment using quantum chemistry methods, all our vibrational calculations already include anharmonicities. Thereby the CH stretching vibrational calculations are presented without any empirical scaling. The dipole moments for the cations are calculated using the center of mass as the origin. The validity of using the local mode model is provided in the ESI,† where we have compared the local mode model results with coupled 4-dimensional vibrational calculations including bending modes.

III. Results and discussions

A. Vibrational spectra of neutral diethyl ether and diethyl sulfide

The experimental spectra of neutral DEE and DES are given in Fig. 1 while in Fig. 2(a), (f) and (g) we present the schematic structure of the stable conformers of neutral DEE and DES, respectively. In both cases the planar anti–anti (aa) conformer

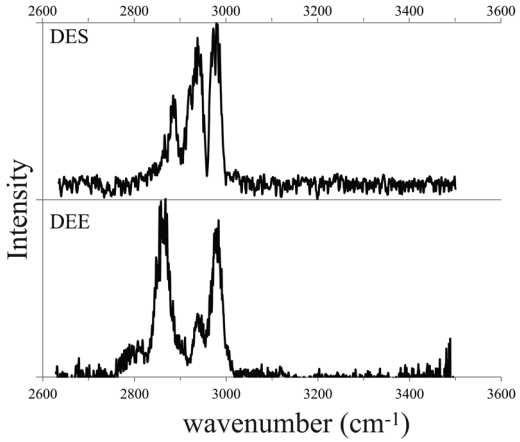

Fig. 1 Experimental spectra of neutral diethyl ether (DEE) and diethyl sulfide (DES) in the 2600–3500 cm^{-1} region.

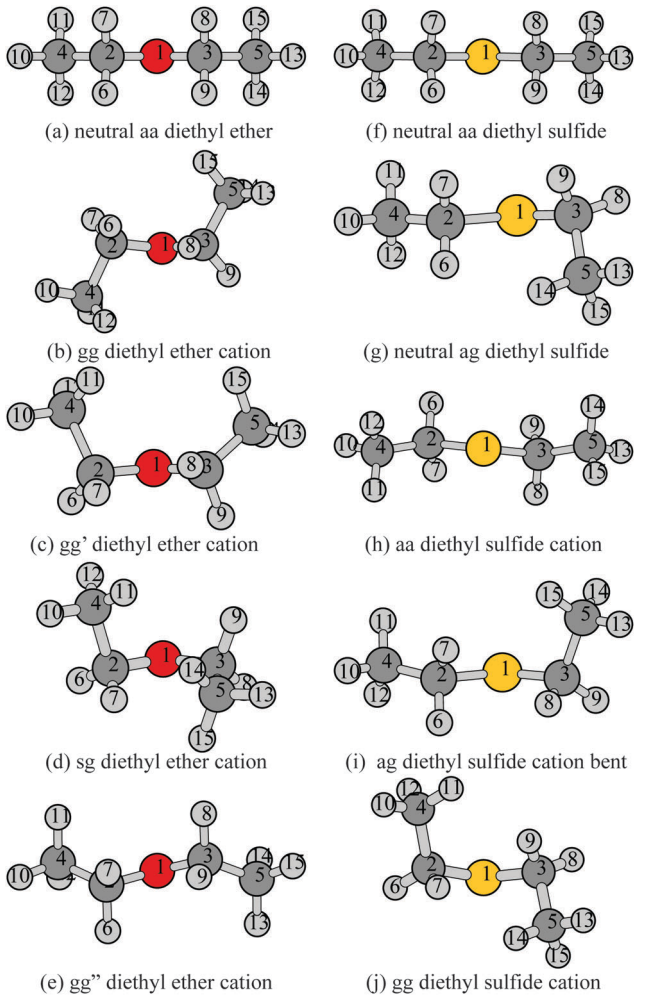

Fig. 2 Schematic diagram of (a) aa diethyl ether, (b) gg diethyl ether cation, (c) gg′ diethyl ether cation, (d) sg diethyl ether cation, and (e) gg″ diethyl ether cation, (f) aa diethyl sulfide, (g) ag diethyl sulfide, (h) aa diethyl sulfide cation, (i) ag diethyl sulfide cation, and (j) gg diethyl sulfide cation.

Table 1 Theoretical peak position, in cm^{-1}, and intensity, in km mol^{-1}, of CH stretching vibration of neutral aa diethyl ether (DEE) and aa diethyl sulfide (DES) calculated using the local mode model with B3LYP/6-31++G(d,p). The experimental peak positions taken from Fig. 1 are also given. See Fig. 2 for the definition of the CH bonds

		C2H6	C4H10	C4H11
aa DEE				
Theory	Peak position	2863	2986	2995
	Intensity	74.8	36.0	26.5
Experiment	Peak position	2860	2980	
aa DES				
Theory	Peak position	2945	2978	2989
	Intensity	38.5	45.2	23.9
Experiment	Peak position	2889/2944		2981

is the most stable, and in Table 1 we report the respective CH local mode (LM) model peak positions and intensities calculated using B3LYP/6-31++G(d,p), as well as the experimental peak maximum. We note that only three CH bonds are given since others are symmetrically equivalent to these three for the aa conformer. We note that for DEE, the anti-gauche (ag) conformer is 1.6 kcal mol^{-1} (at B3LYP/6-31++G(d,p) level) higher in energy compared to the aa conformer. However, for DES the energy difference is only 0.1 kcal mol^{-1} at the B3LYP/6-31++G(d,p) level. Therefore, for DES we also calculated the peak position and intensity for ag DES (see ESI,† Table S5).

Considering that we have two types of CH bonds those bound to the CH_2 group near the oxygen/sulfur and those in the methyl terminal, generally speaking we expect to see two peaks in the CH stretching region. We can see good agreement between the theory (Table 1) and experiment for DEE (Fig. 1 bottom panel), where the peaks in the lower energy 2860 cm^{-1} region are assigned to the CH bonds close to the ether oxygen, while those at higher frequencies, around 2980 cm^{-1}, are assigned to the methyl terminal. To confirm that the coupling between the 4 CH bonds adjacent to the oxygen is small for DEE, we also performed 4-dimensional vibrational calculations. As given in the ESI,† Table S6, the coupling causes the 4 equivalent CH bonds to split, but their splitting between the two most intense peaks are less than 20 cm^{-1}, and are within the peak width of the experimental spectrum. These splitting are due to the symmetric and asymmetric CH stretching modes in the equivalent CH_2 groups. The key point here is that the splitting caused by the couplings are much smaller than the peak position differences between the CH bonds adjacent to the oxygen and methyl terminals.

In the DES experimental spectrum, Fig. 1 upper panel, we observe three peaks rather than two dominant peaks in the case of DEE. On the other hand, the theoretical DES peak position difference between the CH adjacent to the sulfur and on the methyl terminals is within 50 cm^{-1}. So in the case of DES we believe that all 10 CH bonds couple to give these three peaks. This was confirmed by observing the normal modes, and performing anharmonic normal mode calculations using the vibrational perturbation method[62,63] (see ESI,† Table S7). According to these perturbation calculations, in DES, the high energy peak can be assigned to mainly the methyl CH stretching, while the middle peak to mainly the A_1/B_1 CH stretching of the four CH bonds adjacent to sulfur, and lastly the low energy peak to mainly the B_2 CH stretching of the CH bonds adjacent to sulfur. Furthermore, the coupling between the CH stretching fundamental with the HCH bending overtones can also complicate the spectra in this wavenumber region. Indeed, we suspect that the small hump seen between the two peaks in DEE may arise from this Fermi resonance interaction. However, the calculation on this Fermi resonance would require a variational calculation with at least 4 stretching modes and 2 bending modes which is beyond the scope of this paper. The general agreement in the experimental and calculated LM results gives us confidence in using LM calculations with the B3LYP/6-31++G(d,p) method to perform vibrational calculations for the cation species reported in the next section. (More detailed comparison of the LM and LM-4D is given in the ESI,† Table S6.)

B. Vibrational spectra of diethyl ether and diethyl sulfide cations

In Fig. 2(c)–(e) and (g)–(j), we present the schematic diagram of the four lowest energy conformers obtained for DEE^+ and DES^+, respectively. The associated adiabatic ionization energies defined as the relative energies of cationic conformers with respect to the most stable conformer for each neutral species are given in Tables 2 and 3. We note here that for DEE and DEE^+ we performed harmonic calculations to determine the effect of the zero point correction. As seen in Table 2, since these corrections do not greatly alter the relative energetics, we only discuss the electronic energies for the DES system. From the calculated energetics, all the cation conformers that we obtained are all energetically accessible upon 10.5 eV excitation performed in our experiment.

Interestingly, for DEE^+ we obtain structures where the methyl terminal is largely twisted from the planar structure while for DES^+ one of the conformers is fairly close to the planar structure. This difference in optimized cation structure as well as the shape of the cation potential energy surface, given later, originates from the difference in the interaction of the ionized oxygen (sulfur) lone pair orbital with the occupied CH orbitals. First, note that for DEE^+ we found four conformers using PBE0 and MP2, while only three were found using B3LYP. As can be seen in Table 2, the three DEE^+ structures are calculated to be nearly isoenergetic and for convenience we will use the names gauche gauche (gg), gauche gauche′ (gg′), syn gauche (sg), and gauche gauche″ (gg″) to label the structures given in Fig. 2(b)–(e). We note that the geometry optimization using B3LYP, starting with the PBE0 optimized gg″ geometry, ended up in the gg minimum. For the three isoenergetic DES^+ (see Table 3) we will use the names anti anti (aa), anti gauche (ag) and gauche gauche (gg) for the structures in Fig. 2(h)–(j). It is obvious that for both DEE^+ and DES^+ the conformers are related to each other by the rotation of the two CXCC dihedral angle where X = O or S. As shown in the last row in Table 2, the experimental value of 9.52 eV[64] is very close to the results obtained by the single point

Table 2 Ionization energies, in eV, of diethyl ether calculated using several different quantum chemistry methods, as well as the experimental value from NIST database. See Fig. 2 for naming of the structure

Method	gg cation[a]	gg′ cation[a]	sg cation[a]	gg″ cation[a]	Vertical[b]
B3LYP/6-31++G(d,p)	9.22 (9.27)	9.22 (9.29)	9.26 (9.34)		9.55
MP2/6-311++G(3df,3pd)	9.88 (9.92)	9.89 (9.95)	9.94 (10.00)	9.91 (10.0)	10.18
CCSD(T)/6-311++G(3df,3pd)//MP2[c]	9.53	9.56	9.61	9.60	9.84
Experimental[d]	9.52				

[a] Zero point corrected values at the respective levels of calculation methods, electronic energy differences are given in parentheses. [b] Electronic energy difference between the neutral and cationic species at the equilibrium geometry of the neutral species at the respective level. [c] Single point CCSD(T)/6-311++G(3df,3pd) energy calculation using MP2/6-311++G(3df,3pd) geometries. [d] Ref. 64.

Table 3 Ionization energies, in eV, of diethyl sulfide calculated using several different quantum chemistry methods. See Fig. 2 for the naming of the structures

Method	aa cation[a]	ag cation[a]	gg cation[a]	Vertical[a]
B3LYP/6-31++G(d,p)	8.33	8.34	8.36	8.41
CCSD(T)/6-311++G(3df,3pd)//MP2[b]	8.36	8.36	8.37	8.44

[a] Electronic energy differences at the respective levels of calculation methods. [b] Single point CCSD(T)/6-311++G(3df,3pd) energy calculation using MP2/6-311++G(3df,3pd) geometries.

calculation with CCSD(T) using the MP2 geometries. Furthermore, since the T1 diagnostic of Lee *et al.*[65] gave small values (less than 0.02) for all conformers, we believe that the accuracy of the single reference methods is sufficient for this problem.

The experimental vibrational spectra of the cation species of DEE^+ and DES^+ as well as their Ar-tagged 1 : 1 complexes are shown in Fig. 3. First, we compare the bare *versus* the Ar-tagged spectra and then move on to discuss the differences between the DEE^+ and DES^+ systems. The primary difference between DEE^+ and DEE^+–Ar is the width of the red shifted peak seen at $\sim$2700 cm^{-1} and the clear appearance of the CH stretching peak at $\sim$3020 cm^{-1} for the Ar-tagged complex. For DES^+, similarly the peak at the low energy region, 2860 cm^{-1} greatly reduces its band width and a new peak is observed at 3008 cm^{-1} with Ar-tagging. For both cations, new peaks emerge at $\sim$3000 cm^{-1} after Ar-tagging. Since the ionization proceeds through excitation by $\sim$10.5 eV photons, the bare DEE^+ (DES^+) is rather hot with excessive energy in the cationic state. On the other hand, the Ar-tagged complex is fairly cold and possibly trapped in the low energy minima, either in the gg′ or gg″ (aa or ag) forms. Thereby we believe that internal rotation of the methyl groups of the two cations makes it hard to observe these peaks which, as shown later, are assigned to the terminal methyl CH stretching vibrations.

To gain a deeper understanding of the bare cation dynamics, we present the potential energy surface (PES) using B3LYP/6-31++G(d,p) along the two torsion angles corresponding to the ethyl rotation around CXC (X = O or S) in Fig. 4. We calculated energies for dihedral angles in 10 degree grids for C2O1C3C5 and C3O1C2C4 and optimized all other coordinates. Similar figures for MP2 and PBE0 are given in the ESI,† Fig. S1 and they show similar trends. In Fig. 4, we also present the location corresponding to the gg″ minima and one can see that on the B3LYP PES gg″ easily transfers to the gg conformer. It is very interesting to compare the differences in the neutral and cationic PES values for DEE, where the minima for the neutral DEE become a barrier, in the cationic state (see Fig. 4(a) and (b)). On the other hand, DES does not show such a drastic change in the PES by ionization (see Fig. 4(c) and (d)). Furthermore, we also

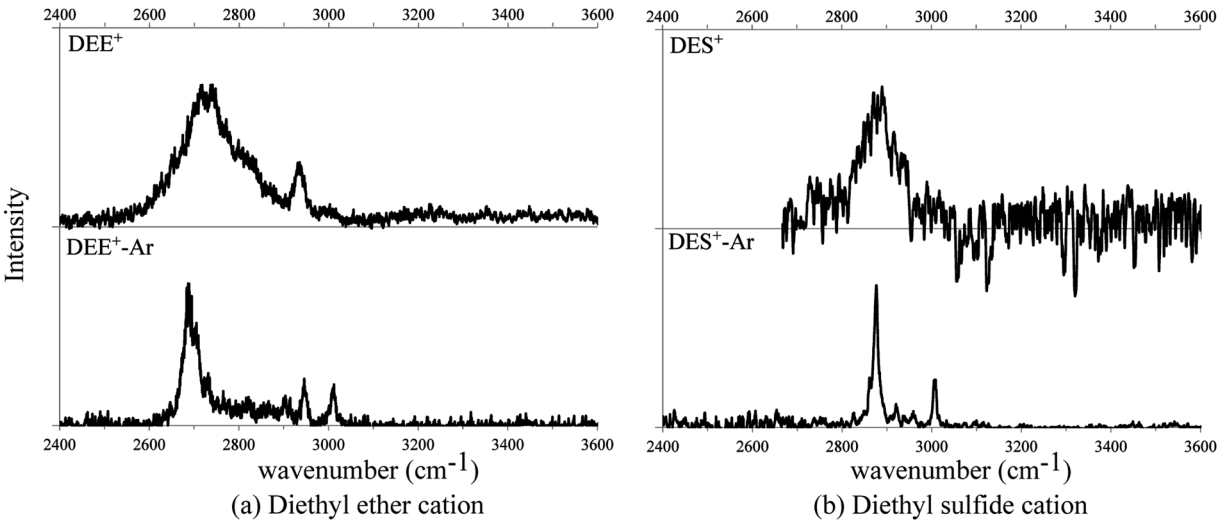

Fig. 3 Experimental spectra of the (a) diethyl ether cation with and without Ar, and (b) the diethyl sulfide cation with and without Ar in the 2500–3600 cm^{-1} region.

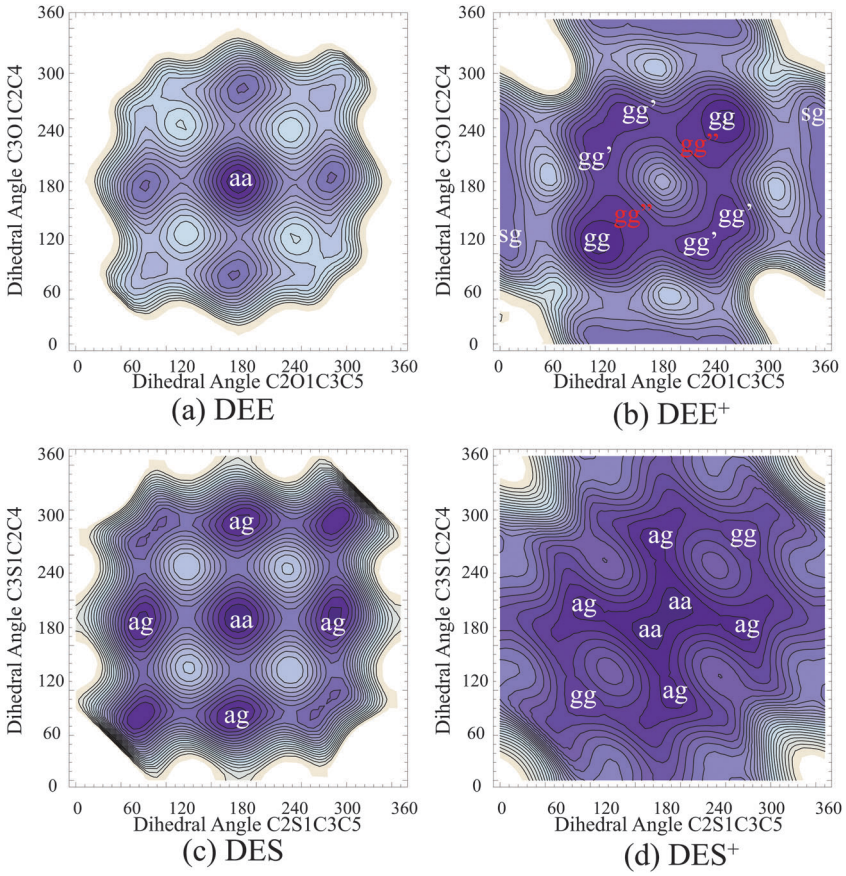

Fig. 4 Two-dimensional potential energy surface for the torsion motion of the ethyl group for (a) diethyl ether, (b) diethyl ether cation, (c) diethyl sulfide, and (d) diethyl sulfide cation. All calculations were performed by fixing the two dihedral angles and optimizing all other coordinates using the B3LYP/6-31++G(d,p) method. The minima are labeled using the names given in Fig. 2–4. Each contour line corresponds to 0.01 eV, and the darker the plot, the lower the energy.

performed on-the-fly direct dynamics following ionization by sampling the zero point vibration geometries of the neutral molecule and initiating the cation calculation from these geometries and kinetic energies. This trajectory mimicking a Franck–Condon ionization is provided in the ESI.† For DEE^+ (see ESI,† DEE.mov), we can observe freely rotating ethyl groups around the COC plane. For DES^+ (see ESI,† DES.mov), the changes in the CSCC dihedral angle are small, but it still rotates around the CSC plane. On the other hand, the terminal methyl groups rotate freely for both cations. We believe that this situation for the hot bare DEE^+ and DES^+ makes it hard to experimentally observe the peak at $\sim$3000 cm^{-1} for both species.

Now looking at the experimental peak positions, while DEE^+ has a strongly red shifted CH peak in the 2700 cm^{-1} wavenumber region, it is absent in the case of DES^+. As can be seen from the theoretical results in Table 4, for gg′ DEE^+ the C3H9 vibration is predicted to have a large red shifted peak at 2766 cm^{-1} with a very large absorption intensity. On the other hand, the lowest peak position predicted for DES^+ is 2908 cm^{-1} for C2H6 and C3H8, thereby the theoretical results also reproduce the experimental observation. To confirm that the LM is sufficient for these cations we also performed LM-4D vibrational calculations for the 4 CH bonds near the oxygen for gg, gg′ and sg using B3LYP/6-31++G(d,p). Similar to the neutral DEE results, the effect of coupling between the CHs is very small and splitting is buried in the width of the experimental spectra (see ESI,† Tables S8–S10). One may also question the effect of the CH bending motion toward the calculated peak positions. Therefore, for gg′ DEE^+ we performed an effective 4D vibrational calculation including the C3H8/C3H9 stretching and H8C3H9 bending modes. From these 4D calculations the C3H9 and C3H8 stretching modes were calculated to show up at 2718 and 2965 cm^{-1}, respectively. They are red shifted by about 40 cm^{-1} compared to the 2765 and 2986 cm^{-1} obtained from the simple LM calculations, and are closer to the experimental peak at 2700 cm^{-1}. The calculation results clearly state that the general trend is obtained by the LM calculations, and red shifts can be attributed to the local changes in the CH bond. See the ESI† for further details concerning these coupled vibrational calculations. Since no other strong peaks are expected in this spectral region, in our previous paper,[27] we assigned the most red shifted CH stretching peak in DEE^+ to the C3H9 stretching motion for gg′.

As mentioned above, due to excess energy as well as the shape of the cationic PES, DEE^+ (DES^+) has enough energy to rotate around the OC (SC) axis as well as the CC axis. As shown

Table 4 Theoretical peak position, in cm^{-1}, and intensity, in km mol^{-1}, of CH stretching vibration of gg and gg′ diethyl ether (DEE^+) and aa and ag diethyl sulfide (DES^+) cations calculated using the local mode model with B3LYP/6-31++G(d,p). Experimental peak positions for the Ar-tagged complex, extracted from Fig. 3, are also given

		C2H6	C2H7	C3H8	C3H9	C4H10	C4H11	C4H12	C5H13	C5H14	C5H15
DEE^+											
gg	Peak	3015	2955	3015	2958	3003	3051	3035	3003	3051	3035
	Int	0.7	30.3	0.7	29.4	13.8	0.2	1.7	14.0	0.2	1.7
gg′	Peak	2958	3013	2982	2766	3003	3036	3053	3019	3031	3014
	Int	31.0	0.5	3.4	168.5	14.7	1.8	0.2	0.7	0.8	4.7
sg	Peak	2930	3062	2836	2817	3007	3035	3052	3015	3003	2996
	Int	38.5	0.6	110.9	104.2	10.3	2.1	0.2	0.5	5.7	5.5
Exp	Peak	2960			2700	3010					
DES^+											
ag	Peak	2913	2942	3006	2992	3012	3020	3017	3001	3025	3020
	Int	23.4	11.8	1.1	4.7	0.3	3.8	3.1	2.6	2.6	6.2
aa	Peak	2908	2958	2908	2958	3013	3021	3017	3012	3021	3017
	Int	24.2	9.6	24.2	9.6	0.3	4.0	3.2	0.3	4.0	3.2
gg	Peak	3006	2997	3006	2997	3001	3020	3026	3001	3020	3027
	Int	3.8	1.2	3.8	1.2	2.5	6.4	2.9	2.5	6.4	2.9
Exp	Peak	2890					3020				

in Fig. 4, the former causes the rotation going from one conformer to another, *i.e.* gg ↔ gg′ ↔ gg″ or aa ↔ ag, while the latter results in the methyl internal rotation. On the other hand, the Ar tagged complex should be cooled down to one of the minima. To determine the effect of these rotations toward the C3H9 stretching vibration, we performed partial optimization along the C2X1C3H9 (X = O, S) dihedral angle, where all internal coordinates, other than the C4C2X1C3 dihedral angle, were optimized. The C4C2O1C3 (C4C2S1C3) dihedral angle was kept constant at 104° (164°), the value at gg′ (aa), so that we could allow just one ethyl branch to rotate. This is equivalent to taking a one-dimensional cut along one of the axes in Fig. 4. Using the optimized geometries, we performed the local mode model vibration calculation for C3H9 at each dihedral angle. At each C2X1C3H9 angle, we solve the one-dimensional vibrational Schrödinger equation for the C3H9 bond using the same protocol used above for the equilibrium geometries: we perform single point calculations for different C3H9 bond lengths using B3LYP to obtain the potential energy and dipole moment. The dihedral angle dependence of the C3H9 vibration as well as the relative energy of the cation for DEE^+ and DES^+ is given in Fig. 5. We note here that the axis for Fig. 5 is given for the CXCH dihedral angle (X = O or S) and if one were to compare with Fig. 4 one should subtract by ∼120° to convert it to the CXCC dihedral angle. As shown in Fig. 5(a), for DEE^+, a large red shift occurs when the C3H9 bond is perpendicular to the COC plane (90 and 270°), while a blue shift compared to the neutral species is seen when C3H9 is in the COC plane (0, 180 and 360°). Similar trends can be seen for DES^+ in Fig. 5(b), but its variation as a function of the dihedral angle is much smaller than DEE^+. We also performed similar partial optimization for the C5 methyl rotation, but the variation of the C3H9 vibrational wavenumber toward methyl rotation was less than 20 cm^{-1} (see Fig. S4 of the ESI†). We note that the dihedral angle dependence of the C3H9 stretching vibration intensity for DEE^+ and DES^+ shows an anti-correlation with its peak

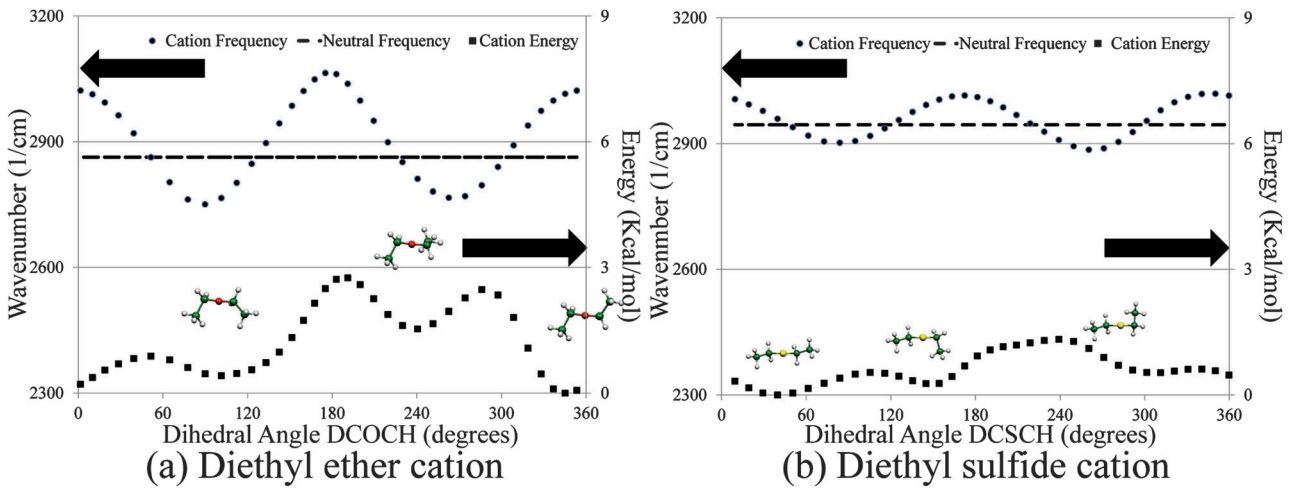

Fig. 5 C2X1C3H9 X = O, S dihedral angle dependence of the energy (squares), in kcal mol^{-1}, and the C3H9 stretching peak position (circles), in cm^{-1}, for (a) diethyl ether and (b) diethyl sulfide cations. The peak position for the neutral C3H9 stretching vibration is given in the dashed line.

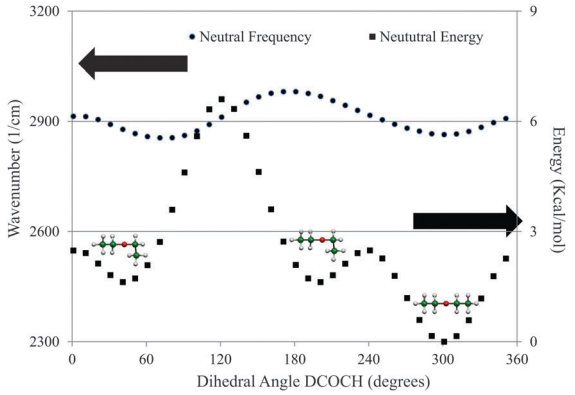

Fig. 6 C2O1C3H9 dihedral angle dependence of the energy (squares), in kcal mol^{-1}, and the C3H9 stretching peak position (circles), in cm^{-1}, for neutral diethyl ether.

position, where a large intensity is seen at 90/270°, while it is nearly zero at 0/180°(see Fig. S5 in the ESI†). As shown in Fig. 6, the C3H9 stretching peak position of the neutral DEE does not show such a large dihedral angle dependence. In the DEE$^+$ experiment, it is likely that most of the conformers are in the most stable gg conformation, but some are trapped in the gg′ conformation accounting for the red shifted peak at 2700 cm^{-1}. For DES$^+$, due to the similarity in the energies it is hard to properly predict which isomers are present in the experiment. However, as seen in Table 4, the ag and aa isomers have strong peaks at 2913 and 2908 cm^{-1}, respectively. On the other hand, gg DES$^+$ does not have such red shifted peaks. Due to the presence of the peaks at ~2890 cm^{-1} in the DES$^+$ and DES$^+$–Ar experimental spectra, we think that the ag or aa isomers are present in the experiment. As a conclusion, these calculations for different isomers show that the relative angle with respect to the C2X1C3 (X = O or S) plane greatly affects the bond strength as well as the polarity of the C3H9 bond. Since the bond strength and polarity along the C3H9 bond is determined by the electron interaction of the σ_{C3H9} orbital with the rest of the molecular orbitals, we resort to Weinhold's NBO analysis[33] to determine the quantitative extent of hyperconjugation in these species.

C. Natural bond orbital analysis on electron delocalization and the CH stretching peak position

Using the NBO analysis, one is able to calculate the non-Lewis interactions that stabilize an occupied bond orbital through the delocalization to an unoccupied orbital. In Fig. 7, we present the hyperconjugation interaction energy between the σ_{C3H9} orbital and the SOMO oxygen/sulfur p orbital for the cations. They showed large variance with respect to the C2X1C3H9 (X = O or S) dihedral angle. We note here that previous studies report that the NBO analysis may overestimate the extent of the hyperconjugation so here we will just compare general trends. For DEE$^+$, at perpendicular geometries, 90/270°, the interaction energy is as great as 15 kcal mol^{-1}, while it is negligible at parallel geometries, 0/180°. Furthermore, one can notice a clear correlation between the $\sigma_{CH} \rightarrow$ O 2p interaction and the C3H9 bond length, where greater the hyperconjugation out of the σ_{CH} orbital the longer the bond. It is well known that the CH bond length is inversely correlated to the CH stretching peak position; thus, this feature also explains the red shift for DEE$^+$. This delocalization also affects the relative conformer energies thereby stabilizing the non-planar forms for DEE$^+$ in Fig. 4(b). One would expect the gg′ conformation to have large steric repulsion compared to gg, thereby making it less stable. However they are isoenergetic because at the gg′ geometry the CH bond can be nearly perpendicular to the COC plane allowing for large hyperconjugation, while in the gg geometry the CH bonds are closer to being in the COC plane (this is because the CC bonds are close to being perpendicular to the COC plane in gg), thus having small electron delocalization. A similar dihedral angle dependence exists for DES$^+$ but the interaction energy at 90/270° is about one-third of that of DEE$^+$, thereby its effect is fairly small. Thus, only a 100 cm^{-1} difference is seen between gg and ag/aa isomers for the peaks corresponding to the CH stretching vibration adjacent to sulfur (see Table 4).

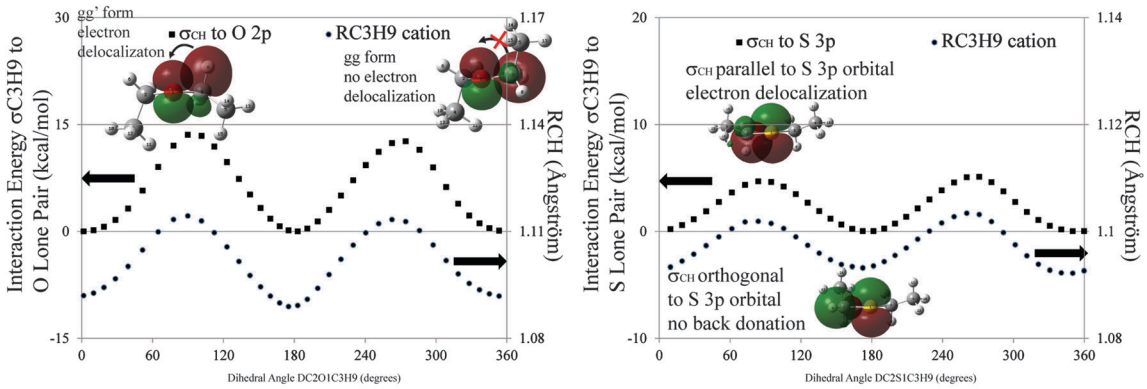

(a) Diethyl ether Cation (b) Diethyl sulfide Cation

Fig. 7 C2X1C3H9 (X = O, S) dihedral angle dependence of the orbital stabilization energy (squares) by the electron delocalization from the σ_{CH} to the O/S p orbitals, in kcal mol^{-1}, and the C3H9 bond length (circles), in Å for (a) diethyl ether and (b) diethyl sulfide cations. Schematic figures of the interacting orbitals are given for 101° and 345° for DEE$^+$ and 101° and 180° for DES$^+$.

As given in the schematic diagrams in Fig. 7, the SOMO is mainly a π symmetry p orbital at oxygen/sulfur with a node at the C2X1C3 plane (X = O or S), thereby when the σ_{CH} orbital is perpendicular to the CXC plane hyperconjugation is large, while it is negligible when it is parallel. The importance of orbital alignment has been previously mentioned for hyperconjugation in hydrocarbon cations.[1,2,24,25] The main reason that this effect is smaller for DES^+ lies in the fact that the orbital energies are more separated for the sulfide case compared to the ether case, *i.e.* the energy of σ_{CH} is much closer to O 2p than S 3p. Furthermore, the CO bond length (~1.4 Å) is much shorter than the CS bond length (~1.8 Å). It is important to note that this interaction is weak for neutral DEE because O 2p is doubly occupied and the delocalization is suppressed. As mentioned by Gussoni *et al.*, in neutral DEE, the delocalization from the lone pair of oxygen to the antibonding orbital of the CH bond causes the bond strength of the CH bonds adjacent to oxygen to weaken.[31] For these cations, the decrease in the electron density from the σ_{CH} orbital results in a more polar CH bond which leads to a larger CH bond dipole moment and a larger vibrational intensity for the stretching vibration of the CH bond adjacent to the oxygen (sulfur) in gg′ DEE^+ (aa/ag DES^+). As a conclusion we see great differences in hyperconjugation interaction that manifests in a drastic difference in the potential energy landscape and the vibrational spectra for DEE^+ *versus* DES^+. This dominance of the $\sigma_{CH} \rightarrow$ 2p/3p hyperconjugation is completely different from the trends seen for the neutral species, and is only active due to ionization from the nonbonding orbital of the oxygen/sulfur atom.

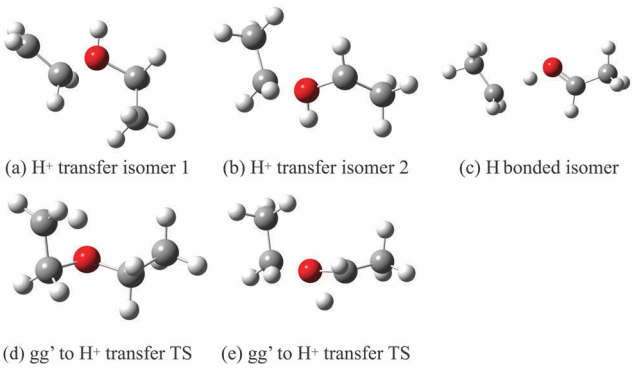

Fig. 8 Schematic diagram of the (a) proton transfer isomer 1 of DEE^+, (b) proton transfer isomer 2 of DEE^+, (c) the hydrogen bonded complex, (d) the transition state connecting gg′ DEE^+ to the proton transfer isomer 1 and (e) the transition state connecting gg′ DEE^+ isomer to proton transfer isomer 2.

D. Possibility of proton transfer from the CH bond

As mentioned above, the CH bond adjacent to the oxygen for DEE^+ is weaker and more polar compared to that of DES^+. Therefore the possibility of intramolecular proton transfer is likely for the former. Indeed, there have been several studies on efficient proton transfer from the CH bond adjacent to the ionized oxygen in methanol,[26] methanol dimer[66] and dimethyl ether[67] cations. Thus we also searched for the proton transferred isomer for DEE^+ and found two alcohol structures given in Fig. 8(a) and (b). Isomer 1, given in Fig. 8(a) is obtained from the proton transfer from the terminal methyl group of gg′ while isomer 2 given in Fig. 8(b) is obtained from the transfer from the CH adjacent to the oxygen. For isomer 2, the strong interaction between the radical on CH_2CH_3 and the proton on the alcohol allows for a hydrogen bonded isomer given in Fig. 8(c). Looking at the energies given in the first three columns of Table 5, one will notice that the hydrogen bonded complex is isoenergetic to the gg isomer (see Table 2). Similarly, thiol structures were also obtained for DES^+, and the structures are given in the ESI,† Fig. S6. For DES^+, from the energetics given in Table 5, one can notice that the thiol isomers as well as their hydrogen bonded complex is 0.8 eV higher in energy compared to the aa and ag isomers (see Table 3). This is consistent with the higher acidic character of CH in DEE^+ compared to DES^+. Furthermore, this signifies the stronger proton affinity of oxygen compared to sulfur in the cationic state. From the energetics given in Table 5, one may expect that these alcohol/thiol isomers may exist under the experimental conditions of 10.5 eV excitation from neutral DEE. As can be seen from the transition state barrier energies for these intramolecular proton transfer, given in the last two columns of Table 5, we believe that it will not be easy for the proton transfer reaction to occur in DEE^+. In addition, the most intense OH stretching fundamental peaks for the proton transferred isomers 1, 2 and the hydrogen bonded complex were calculated to be 3516, 3524 and 1254 cm^{-1}, respectively, using the local mode model with B3LYP/6-31++G(d,p). As for DES^+, the transition state energies, given in Table 5, are below 10.5 eV excitation used

Table 5 Relative electronic energies, in eV, of diethyl ether cation alcohol isomers and diethyl sulfide cation thiol isomers calculated using several different quantum chemistry methods. See Fig. 8 and Fig. S6 in the ESI for naming of the structures. Zero of energy is neutral diethyl ether/diethyl sulfide calculated at the respective levels of quantum chemistry

Method	H^+ transfer 1	H^+ transfer 2	H bonded 1	Transition state 1	Transition state 2
DEE^+					
B3LYP/6-31++G(d,p)	9.46	9.52	9.24	10.63	10.83
CCSD(T)/6-311++G(3df,3pd)//MP2[a]	9.48	9.57	9.45	10.74	10.95
DES^+					
B3LYP/6-31++G(d,p)	9.16	9.15	9.20	9.93	10.17
CCSD(T)/6-311++G(3df,3pd)//MP2[a]	9.14	9.12	9.53	9.92	10.16

[a] Single point CCSD(T)/6-311++G(3df,3pd) energy calculation using MP2/6-311++G(3df,3pd) geometries.

in the experiment; thus energetically proton transfer is possible. For these thiol isomers we also calculated the peak positions of the SH stretching vibrations. The fundamental peak position for the proton transferred isomers 1, 2 and the hydrogen bonding complex were calculated to be 2560, 2538, and 2050 cm^{-1}, respectively, using local mode model with B3LYP/6-31++(d,p). Since we do not observe strong peaks in the experiment for DEE^+, DES^+ and their Ar-tagged species in these regions (see Fig. 3), we think that their existence is minimal. We note that recently a proton transfer from the CH bond in dimethyluracil dimer[68] as well as trimethylamine dimer[69] was observed following ionization and we also observed a proton transfer from the CH bond adjacent to the oxygen in $(DEE)_2^+$.[70] Therefore, the acidity of the CH bonds adjacent to the ionized SOMO of nitrogen and oxygen can be said to be fairly large.

IV. Conclusion

We presented experimental spectra of the diethyl ether cation which showed a strong red shifted CH stretching peak at 2700 cm^{-1}. On the other hand, for the diethyl sulfide cation and the neutral species such a strong red shifted peak was absent. Using quantum chemistry methods and local mode vibrational calculations we confirmed that only DEE^+ will have an intense red shifted peak. Furthermore, this red shifted peak is assigned to the CH bond adjacent to the oxygen which is nearly perpendicular to the COC plane. Utilizing the natural bond orbital analysis, we provided a simple rationalization through the difference in the hyperconjugation electron delocalization of the σ_{CH} orbital to the SOMO p orbital of oxygen/sulfur for the cation species. Since the SOMO has a node at the COC plane, the maximum hyperconjugation occurs when the σ_{CH} orbital is perpendicular to the plane, thus accounting for the large red shift. Similar sensitivity of the peak position with respect to the angle of the CH bond *versus* the CSC plane was seen for DES^+, but its effect was about one-third of that of DEE^+. Interaction with oxygen is stronger than sulfur due to the smaller energy difference between the p orbital and the σ_{CH} orbital. In addition, the shorter CO distance in DEE compared to the CS distance in DES also contributes to the stronger interaction in the former. This hyperconjugation explains the drastic change in the DEE potential energy surface following ionization, which is absent in DES. For DEE, DES and DES^+, the steric repulsion dominates favoring the geometry in which the two terminal methyl groups are far in distance. On the other hand, for DEE^+, the strong hyperconjugation interaction stabilizes geometries where steric repulsion is large. For gg′ DEE^+, by having CH bonds nearly perpendicular to the COC plane the σ_{CH} orbital interacts strongly with its adjacent ionized SOMO oxygen p orbital. This study showed how orientation with the ionized orbital can greatly affect the neighboring CH bond strength and its polarity, as well as the stable geometry of the system. Furthermore, we studied the possibility of the intramolecular proton transfer in these systems. From the detailed comparison of the experimental and theoretical results we conclude that with the 10.5 eV ionization scheme used in the present set up such intramolecular proton transfer is unlikely.

Acknowledgements

YM acknowledges support from the Sumitomo Foundation and the Grant-in-Aid for Scientific Research (Project No. 26108504 on Innovative Area [2507]) from MEXT Japan. AF acknowledges the Grant-in-Aid for Scientific Research (Project No. 26288002) from JSPS. KT thanks Academia Sinica, National Center for High Performance Computing and Ministry of Science and Technology (NSC 102-2113-M-001-012-MY3) of Taiwan for support.

References

1 R. S. Mulliken, *J. Chem. Phys.*, 1939, **7**, 339.
2 R. S. Mullliken, C. A. Rieke and W. G. Brown, *J. Am. Chem. Soc.*, 1941, **63**, 41.
3 I. V. Alabugin, K. Gilmore and P. Peterson, *WIREs Comput. Mol. Sci.*, 2011, **1**, 109.
4 T. K. Brunck and F. Weinhold, *J. Am. Chem. Soc.*, 1979, **101**, 1700.
5 V. Pophristic and L. Goodman, *Nature*, 2001, **411**, 565.
6 P. R. Schreiner, *Angew. Chem., Int. Ed.*, 2002, **41**, 3579.
7 F. M. Bickelhaupt and E. J. Baerends, *Angew. Chem., Int. Ed.*, 2003, **42**, 4183.
8 Y. Mo, W. Wu, L. Song, M. Lin, Q. Zhang and G. Gao, *Angew. Chem., Int. Ed.*, 2004, **43**, 1986.
9 Y. Mo, *Nat. Chem.*, 2010, **2**, 666.
10 W. H. Saunders Jr, *J. Org. Chem.*, 1999, **64**, 861.
11 W. H. Saunders Jr, *J. Org. Chem.*, 2000, **65**, 681.
12 G. Meloni, P. Zou, S. J. Klippenstein, M. Ahmed, S. R. Leone, C. A. Taatjes and D. L. Osborn, *J. Am. Chem. Soc.*, 2006, **128**, 13559.
13 G. Meloni, T. M. Selby, F. Goulay, S. R. Leone, D. L. Osborn and C. A. Taatjes, *J. Am. Chem. Soc.*, 2007, **129**, 14019.
14 S. Okajima, B. T. Lim and E. C. Lim, *J. Chem. Phys.*, 1980, **73**, 3512.
15 H. Vancik, *J. Pure Appl. Phys.*, 1995, **67**, 761.
16 P. D. Jawowski, M. D. Wodrich, C. S Wannere, P. v. R. Schleyer and K. N. Houk, *J. Am. Chem. Soc.*, 2004, **126**, 15036.
17 K. U. Ingold and G. A. DiLabio, *Org. Lett.*, 2006, **8**, 5923.
18 I. Fernandez and G. Frenking, *Chem. – Eur. J.*, 2006, **12**, 3617.
19 H. G. Kjaergaard, A. L. Garden, G. M. Chaban, R. B. Gerber, D. A. Matthews and J. F. Stanton, *J. Phys. Chem. A*, 2008, **112**, 4324.
20 R. M. Badge and S. H. Bauer, *J. Chem. Phys.*, 1937, **5**, 605.
21 R. M. Badge and S. H. Bauer, *J. Chem. Phys.*, 1937, **5**, 839.
22 G. C. Pimentel and A. L. McClellan, *The Hydrogen Bond*, W. H. Freeman, San Francisco, 1960.
23 P. Schuster, G. Zundel and C. Sandorfy, *The Hydrogen Bond II. Structure and Spectroscopy*, North-Holland, Amsterdam, 1976.

24 A. Fujii, E. Fujimak, T. Ebata and N. Mikami, *J. Chem. Phys.*, 2000, **112**, 6275.
25 G. E. Douberly, A. M. Ricks, B. W. Ticknor, P. v. R. Schleyer and M. A. Duncan, *J. Am. Chem. Soc.*, 2007, **129**, 13782.
26 J. D. Mosley, J. W. Young, M. Huang, A. B. McCoy and M. A. Duncan, *J. Chem. Phys.*, 2015, **142**, 114301.
27 Y. Matsuda, T. Endo, M. Morita, K. Takahashi, N. Mikami and A. Fujii, *J. Phys. Chem. A*, 2015, **119**, 4885–4890.
28 V. Hernandez, C. Castiglioni and G. Zerbi, *J. Mol. Struct.*, 1994, **324**, 189.
29 M. Gussoni and C. Castiglioni, *J. Mol. Struct.*, 2000, **521**, 1.
30 C. Castiglioni, M. Gussoni and G. Zerbi, *J. Mol. Struct.*, 1989, **198**, 475–488.
31 M. Gussoni, C. Castiglioni and G. Zerbi, *Handbook of vibrational spectroscopy*, Wiley, London, 2001, pp. 2014–2078.
32 J. P. Foster and F. Weinhold, *J. Am. Chem. Soc.*, 1980, **102**, 7211.
33 A. E. Reed, L. A. Curtiss and F. Weinhold, *Chem. Rev.*, 1988, **88**, 899.
34 Y. Matsuda, N. Mikami and A. Fujii, *Phys. Chem. Chem. Phys.*, 2009, **11**, 1279–1290.
35 A. D. Becke, *J. Chem. Phys.*, 1993, **98**, 5648–5652.
36 C. Lee, W. Yang and R. G. Parr, *Phys. Rev. B: Condens. Matter Mater. Phys.*, 1988, **37**, 785–789.
37 A. D. McLean and G. S. Chandler, *J. Chem. Phys.*, 1980, **72**, 5639–5648.
38 R. Krishnan, J. S. Binkley, R. Seeger and J. A. Pople, *J. Chem. Phys.*, 1980, **72**, 650–654.
39 T. Clark, J. Chandrasekhar, G. W. Spitznagel and P. v. R. Schleyer, *J. Comput. Chem.*, 1983, **4**, 294–304.
40 M. J. Frisch, J. A. Pople and J. S. Binkley, *J. Chem. Phys.*, 1984, **80**, 3265–3269.
41 J. P. Perdew, K. Burke and M. Ernzerhof, *Phys. Rev. Lett.*, 1996, **77**, 3865–3868.
42 J. P. Perdew, K. Burke and M. Ernzerhof, *Phys. Rev. Lett.*, 1997, **78**, 1396.
43 C. Adamo and V. Barone, *J. Chem. Phys.*, 1999, **110**, 6158–6169.
44 C. Moller and M. S. Plesset, *Phys. Rev.*, 1934, **46**, 618–622.
45 R. J. Bartlett and G. D. Purvis III, *Int. J. Quantum Chem.*, 1978, **14**, 561–581.
46 J. A. Pople, R. Krishnan, H. B. Schlegel and J. S. Binkley, *Int. J. Quantum Chem.*, 1978, **14**, 545–560.
47 G. D. Purvis III and R. J. Bartlett, *J. Chem. Phys.*, 1982, **76**, 1910–1918.
48 J. A. Pople, M. Head-Gordon and K. Raghavachari, *J. Chem. Phys.*, 1987, **87**, 5968–5975.
49 J. M. Millarn, V. Bakkenm, W. Chen, W. L. Hase and H. B. Schlegel, *J. Chem. Phys.*, 1999, **111**, 3800.
50 M. J. Frisch, G. W. Trucks, H. B. Schlegel, G. E. Scuseria, M. A. Robb, J. R. Cheeseman, G. Scalmani, V. Barone, B. Mennucci, G. A. Petersson, H. Nakatsuji, M. Caricato, X. Li, H. P. Hratchian, A. F. Izmaylov, J. Bloino, G. Zheng, J. L. Sonnenberg, M. Hada, M. Ehara, K. Toyota, R. Fukuda, J. Hasegawa, M. Ishida, T. Nakajima, Y. Honda, O. Kitao, H. Nakai, T. Vreven, J. A. Montgomery, Jr., J. E. Peralta, F. Ogliaro, M. Bearpark, J. J. Heyd, E. Brothers, K. N. Kudin, V. N. Staroverov, R. Kobayashi, J. Normand, K. Raghavachari, A. Rendell, J. C. Burant, S. S. Iyengar, J. Tomasi, M. Cossi, N. Rega, J. M. Millam, M. Klene, J. E. Knox, J. B. Cross, V. Bakken, C. Adamo, J. Jaramillo, R. Gomperts, R. E. Stratmann, O. Yazyev, A. J. Austin, R. Cammi, C. Pomelli, J. W. Ochterski, R. L. Martin, K. Morokuma, V. G. Zakrzewski, G. A. Voth, P. Salvador, J. J. Dannenberg, S. Dapprich, A. D. Daniels, O. Farkas, J. B. Foresman, J. V. Ortiz, J. Cioslowski and D. J. Fox, *Gaussian 09, Revision A.02*, Gaussian, Inc., Wallingford CT, 2009.
51 R. L. Swofford, M. E. Long and A. C. Albrecht, *J. Chem. Phys.*, 1976, **65**, 179.
52 B. R. Henry, *Acc. Chem. Res.*, 1977, **20**, 207.
53 M. S. Child and R. T. Lawton, *Chem. Phys. Lett.*, 1982, **87**, 217.
54 M. Quack, *Annu. Rev. Phys. Chem.*, 1990, **41**, 839.
55 A. V. Fedorov and D. L. Snavely, *Chem. Phys.*, 2000, **254**, 169.
56 H. G. Kjaergaard, H. Yu, J. S. Bernhard, R. H. Bryan and W. T. Allan, *J. Chem. Phys.*, 1990, **93**, 6239.
57 K. Takahashi, M. Sugawara and S. Yabushita, *J. Phys. Chem. A*, 2002, **106**, 2676.
58 K. Takahashi, M. Sugawara and S. Yabushita, *J. Phys. Chem. A*, 2005, **109**, 4242.
59 J. C. Light, I. P. Hamilton and J. V. Lill, *J. Chem. Phys.*, 1985, **82**, 1400.
60 M. Morita and K. Takahashi, *Phys. Chem. Chem. Phys.*, 2013, **15**, 114.
61 M. Morita and K. Takahashi, *Phys. Chem. Chem. Phys.*, 2013, **15**, 14973.
62 V. Barone, *J. Chem. Phys.*, 2004, **120**, 3059–3065.
63 V. Barone, *J. Chem. Phys.*, 2005, **122**, 014108.
64 *NIST Chemistry WebBook, NIST Standard Reference Database Number, 69, NIST, Chemistry WebBook*, ed. P. J. Linstrom, and W. G. Mallard, National Institute of Standards and Technology, Gaithersburg, MD 20899, 2011, http://webbook.nist.gov.
65 T. J. Lee and P. R. Taylor, *Int. J. Quantum Chem., Quantum Chem. Symp.*, 1989, **S23**, 199.
66 S.-T. Tsai, J.-C. Jiang, Y. T. Lee, A. H. Kung, S. H. Lin and C.-K. Ni, *J. Chem. Phys.*, 1999, **111**, 3434.
67 B. Yonder, K. B. Bravaya, A. Bodi, A. H. C. West, B. Sztaray and R. Signorell, *J. Chem. Phys.*, 2015, **142**, 114303.
68 A. Golan, K. B. Bravaya, R. Kudirka, O. Kostko, S. R. Leone, A. I. Krylov and M. Ahmed, *Nat. Chem.*, 2012, **4**, 323.
69 Y. Matsuda, Y. Nakayam, N. Mikami and A. Fujii, *Phys. Chem. Chem. Phys.*, 2014, **16**, 9619.
70 Y. Matsuda, X. Min and A. Fujii, in preparation.

